Liquid−Vapor Oscillations of Water Nanoconfined between Hydrophobic Disks: Thermodynamics and Kinetics

Limei Xu[†,‡] **and Valeria Molinero***[,†]

Department of Chemistry, University of Utah, 315 South 1400 East, Salt Lake City, Utah 84112-0850, and WPI-Advanced Institute for Materials Research, Tohoku University, 2-1-1 Katahira, Sendai 980-8577, Japan

Received: March 17, 2010; Revised Manuscript Received: April 27, 2010

We use extensive molecular dynamics simulations with the monatomic model of water (mW) to characterize the thermodynamics and kinetics of the liquid−vapor (wetting−drying) equilibrium of water confined between nanoscopic hydrophobic plates. The transition in confined water is first-order-like, with two well-defined states (wet and dry) separated by a free energy barrier. Different from its bulk counterpart, the confined system oscillates between liquid and vapor: the two phases coexist in time but not in space. Also different from the phase behavior in bulk, there is a finite range of the thermodynamic variables (e.g., temperature or separation between the plates) for which the liquid and vapor state coexist in dynamical equilibrium. We determine the range of temperatures and plate separations for which reversible oscillations can be observed between a stable and metastable phase, compute the time scales of the phase transition along the equilibrium coexistence line, and investigate the pathway for drying along simple collective coordinates that describe the opening of a vapor bubble. The results of the simulations are compared with a simple capillary model for the thermodynamics and transition state theory for the kinetics of phase oscillations.

Downloaded via UNIV OF MASSACHUSETTS AMHERST on July 21, 2022 at 21:11:48 (UTC).
See https://pubs.acs.org/sharingguidelines for options on how to legitimately share published articles.

Introduction

Water confined in small nanopores and nanocavities behaves differently than bulk water.[1–6] The phase diagram of bulk water is completely defined by the pressure p and temperature T. Confinement of water in nanoscopic volumes adds new thermodynamic variables (the dimensions of confinement and the water−surface interaction) and increases the richness of its phase behavior: a wealth of novel ice and liquid phases have been reported for water confined in nanopores and nanoslits.[7–20] Confinement also affects the temperature of phase equilibria, turning vapor[5,21–28] or ice[29] into stable phases at ambient temperature, conditions for which the liquid is the only stable phase in bulk water. Particular attention has been paid to the effect of hydrophobic interfaces in dewetting and hydrophobic collapse[1,2,23,25,30–32] and to the structure, thermodynamics, and anomalously fast transport of water through hydrophobic carbon nanotubes.[3,5,26,33] Molecular simulations indicate that minute changes in the strength of water−surface attraction suffice to prevent dewetting of nanopores[26–28] and nanoslits.[21]

Confinement in nanoscopic volumes not only shifts the equilibrium between liquid and vapor but also changes the nature of phase coexistence.[34] Cooperative density oscillations between liquid (wet) and vapor (dry) states have been observed in simulations of water confined in hydrophobic nanopores[5,33] and nanoslits,[21,35] in which the confined system is open to exchange water with a surrounding bath. There is no bulk equivalent for this phenomenon in which fluctuations between two distinct states (far from a critical point) encompass the full size of the confined system.

The focus of the present work is the characterization of the thermodynamics and kinetics of liquid−vapor coexistence and density oscillations in water confined between parallel hydrophobic disks. We use molecular dynamics simulations with a computationally efficient coarse-grained model of water to compute the phase diagram of water confined between hydrophobic disks of radius ∼1 nm in equilibrium with a bath of liquid water at 1 atm and to determine the thermodynamic conditions for which oscillations between the two phases could be observed. The main questions that we address are: What are the thermodynamic conditions (temperature, size, and separation between the plates) for which the nanoconfined liquid and vapor coexist in equilibrium? What is the range of thermodynamic conditions over which dynamical coexistence between a stable and metastable phase can be observed in nanoconfined water? What are the characteristic survival times of the phases in dynamical coexistence? What are good "reaction coordinates" to describe the pathway of the wetting−drying transition between hydrophobic disks? We conclude with a discussion on whether the results presented here for the vapor−liquid transition in water could be generalized to other phase transitions and substances.

Methods

System and Force Fields. The system consisted of two parallel disks of *radius* R_p at a distance D immersed in bulk water, as sketched in Figure 1. Except when otherwise indicated, each of the disks is planar and rigid, conformed by 31 particles arranged in a triangular lattice with particle distance 3.2 Å, leading to $R_p = 8.8$ Å. The simulation cell was periodic and contained 8496 water molecules that freely exchanged between the confined system (the volume between the plates) and the water bath (outside the plates).

Water was modeled with the monatomic model mW that represents each molecule as a single particle with short-range potentials[36]

* Corresponding author. E-mail: Valeria.Molinero@utah.edu.
† University of Utah.
‡ Tohoku University.

10.1021/jp102443m © 2010 American Chemical Society
Published on Web 05/06/2010

$$
\begin{aligned}
E &= \sum_i \sum_{j>i} \phi_2(r_{ij}) + \sum_i \sum_{j\neq i} \sum_{k>j} \phi_3(r_{ij}, r_{ik}, \theta_{ijk}) \\
\phi_2(r_{ij}) &= A\varepsilon\left[B\left(\frac{\sigma}{r_{ij}}\right)^4 - 1\right]\exp\left(\frac{\sigma}{r_{ij} - a\sigma}\right) \\
\phi_3(r_{ij}, r_{ik}, \theta_{ijk}) &= \lambda\varepsilon[\cos\theta_{ijk} - \cos\theta_0]^2\exp\left(\frac{\gamma\sigma}{r_{ij} - a\sigma}\right) \times \\
&\qquad \exp\left(\frac{\gamma\sigma}{r_{ik} - a\sigma}\right)
\end{aligned} \tag{1}
$$

where r_{ij} is the distance between particles i and j and θ_{ijk} is the angle subtended by the vectors between the positions of the $i-j$ and $i-k$ pairs of particles. The constants $A = 7.049556277$, $B = 0.6022245584$, $\gamma = 1.2$, $a = 1.8$, and $\theta_o = 109.5°$ are the same for the mW water model and the Stillinger−Weber silicon potential.[37] The characteristic size for water−water interactions is $\sigma = 2.3925$ Å, and the depth of the two-body interaction potential is $\varepsilon = 6.189$ kcal/mol. The three-body terms ϕ_3 encourage "hydrogen-bonded" configurations in the mW water model by imposing a penalty to configurations with water−water−water angles that depart from the tetrahedral value, $\theta_o = 109.5°$. The value of the parameter $\lambda = 23.15$ determines the strength of the tetrahedral interactions. All intermolecular forces vanish at a cutoff distance $r_c = a\sigma = 4.32$ Å.

The monatomic water model mW is 2 orders of magnitude computationally more efficient than atomistic models of water with Ewald sums,[36] allowing for the long simulation times needed to characterize the transitions between confined liquid and vapor states. Important for this study, the mW model reproduces the structure of liquid water and the essential features responsible for capillary evaporation, such as the enthalpy of vaporization (10.65 kcal/mol in mW compared to 10.52 in experiments) and liquid−vapor surface tension (66 mJ/m^2 in mW and 71.6 mJ/m^2 in experiments, both at 298 K).[36]

The equations of motion of the particles of the rigid plates were not integrated during the simulation. The interactions between plate particles were set to zero to avoid spurious contributions of their forces to the virial. The interaction of water with the particles of the plates was described by a pair potential ϕ_2 with the form and constants of eq 1, except for the characteristic size, $\sigma_{wp} = 3.56$ Å, and the strength of the interactions, $\varepsilon_{wp} = 0.136$ kcal/mol. The topology of the plates and their σ_{wp} and ε_{wp} were the same as in the study of Berne and co-workers in ref 31. These result in hydrophobic plates with a contact angle of $\theta_{wp} \sim 115°$ for mW water.[29]

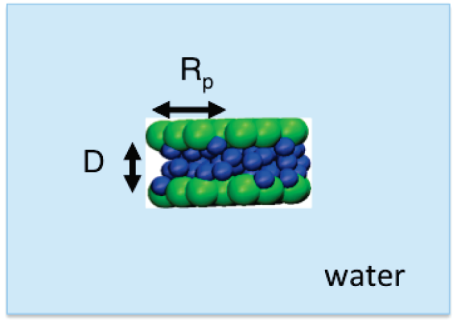

Figure 1. Confined system consisting of water (blue balls) between two nanoscopic disks (green balls) of radius R_p separated by a distance D. The confined system was immersed in a bath of bulk water (represented by a blue shade) and exchanged water molecules with it. In this work, we explore the liquid−vapor equilibrium of the confined water as a function of the distance D and the temperature T, while the pressure of the liquid in the bath is kept at 1 atm.

Simulation Settings. Molecular dynamics simulations of the whole system (water bath, plates, and water confined between them) were performed using LAMMPS.[38,39] The system was simulated with periodic boundary conditions. The equations of motion were integrated with the velocity Verlet algorithm with a time step of 5 fs. *NpT* simulations of the whole system were carried at $p = 1$ atm at temperatures T from 300 to 600 K using the Nose−Hoover thermostat and barostat with damping constants 5 and 25 ps, respectively. Simulation times were 200−400 ns for each T and plate separation D. The number of water molecules outside the plates was 2 orders of magnitude larger than between the plates, thus effectively controlling the chemical potential of water in the confined volume.

Property Calculation. The instantaneous *density* of the confined system was computed as the number of particles within the volume enclosed by the plates, $\rho = N_{confined}/\pi D R_p^2$. The average density of bulk water under the same conditions ρ_o was measured in an analogous way, selecting a slab of bath volume far from the plates and averaging the value over the simulation trajectory.

The *free energy* along a reaction coordinate (e.g., ρ) is the *potential of mean force* (PMF) along that coordinate. The confined water is at conditions of constant $\{\mu,V,T\}$; the characteristic thermodynamic potential for those conditions is the grand canonical free energy Ω. We use the density of water between the plates, ρ, as an order parameter or "reaction coordinate" for the advance of the transformation between vapor and liquid to compute the potential of mean force (PMF) as a function of the order parameter

$$
\Omega(\rho, \{\mu, V, T\}) = -RT \ln P(\rho) \tag{2}
$$

where $P(\rho)$ is the probability of measuring a density ρ for water confined between the plates; R is the universal gas constant; and $\{\mu,V,T\}$ indicate the thermodynamic conditions for water between the plates. For simplicity, we omit the thermodynamic state in the notation that follows.

The *survival probabilities* $P_s(t)$ of the liquid (vapor) were computed from long time series of the confined density $\rho(t)$, where we considered that the liquid (vapor) transitions onto vapor (liquid) every time the system crosses over $\rho^{\#}/\rho_o$ corresponding to the top of the free energy barrier, minus (plus) $\delta(\rho/\rho_o) = 0.03$. The value of $\delta(\rho/\rho_o)$ was chosen to avoid counting the mere reaching of the barrier as a transition event. The characteristic *survival times* τ of the liquid (vapor) states were computed from the fitting of the survival probability to a single exponential, $P_s(t) = C\exp(-t/\tau)$, where $C < 1$ indicates the fraction of trajectories that succeed in transforming into vapor (liquid) after crossing $\rho/\rho_o - (+)\ \delta(\rho/\rho_o)$.

The *area* A and *perimeter* L of the largest vapor bubble between the plates was computed for the characterization of the dewetting process. To compute the area and perimeter of the bubble, we projected the coordinates of all water particles within the plate volume into the plane parallel to the plates and binned the positions in a square grid. Each square bin had a side of $R_p/4 = 2.2$ Å. Then we determined which bins were empty and, if they were connected, added up their area to compute the area A and their sides exposed to filled ones to compute the perimeter L. Only the largest bubble was considered for the analysis. Due to the small dimensions of the system, the approximation of a square grid results in values of L for the vapor state bubbles larger than the $L = 2\pi R_p$ expected for a smooth curve.

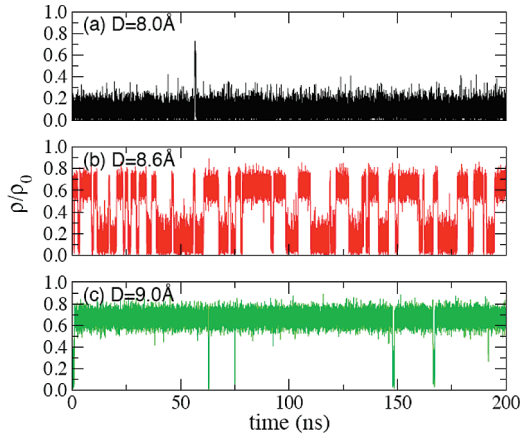

Figure 2. Time evolution of the relative density of water confined between the plates compared to the bulk value for plates with R_p = 8.8 Å at T = 300 K immersed in a bath of liquid water at the same T and p = 1 atm. The relative population of the wet (high density) to dry (low density) states increases as the plates are separated (a to c). Transitions between the two states are observed within a small separation range of approximately 1 Å, between 8.0 and 9.1 Å. It should be noted that the nonzero density of the dry states arises from water molecules at the rim of the plates; the vapor bubble is always empty. (a) For a small separation of 8.0 Å, the dry state predominates. (b) At an intermediate separation of 8.6 Å, frequent transitions between wet and dry are observed. (c) For a larger separation of 9.0 Å, the wet state predominates.

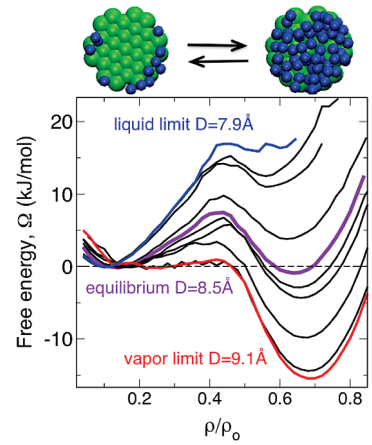

Figure 3. Upper panel: representative configurations of the vapor (also called dry) state (left) and the liquid (also called wet) state (right). For clarity, only one of the plates (green balls) and the water molecules in the volume between the plates (blue balls) are shown. Lower panel: free energy of the phase transition between vapor and liquid at T = 330 K along the reduced density coordinate. The confined system is in contact with a bath of liquid water at 330 K and 1 atm. At fixed temperature T = 330 K, the liquid and vapor states coexist in dynamical equilibrium for plate separations between 7.9 and 9.1 Å. The liquid limit D = 7.9 Å is the smaller plate separation for which the liquid occupies the volume between the plates. The vapor limit D = 9.1 Å is the largest separation for which vapor forms between the plates.

Results and Discussion

We investigate the phase behavior of the water confined between the hydrophobic plates. The thermodynamic state of water confined between the plates is characterized by a constant volume $V = \pi R^2 D$, temperature T, and chemical potential μ (controlled by p and T of water in the surrounding bath). We first focus on the effect of the distance between the plates on the phase behavior of confined water, then analyze the temperature dependence of the liquid−vapor equilibrium and, finally, the kinetics of the phase transformation.

Figure 2 shows the time evolution of the density of water between the plates ρ, normalized by the average density of water in the bath ρ_o, for plate separations D = 8, 8.6, and 9 Å at T = 300 K immersed in a bath of water at the same T and p = 1 atm. As the confined system is open to the bath, the density fluctuates in all cases. The fluctuations occur around two average values that correspond to empty (dry) and filled (wet) plates. These are the nanoconfined analogues of the bulk vapor and liquid phases, respectively. The upper panel of Figure 3 shows snapshots of the dry and wet states. We note that although the average density of the vapor state is around 10% of the bulk liquid value this is only because some water molecules access the rim of the plates (upper left panel of Figure 3); the vapor bubble itself is always empty. In the same way, the density of the liquid seems to be just about 70% of the bath because the excluded volume occupied by the plate particles, inaccessible to the water, is still considered in the calculation of the density.

The wet and dry states are analogous to liquid and vapor in bulk water. Figure 2 shows, however, important differences in the phase behavior of the confined and bulk water:

(i) The vapor phase is stable in the confined system at conditions for which liquid is the stable state of bulk water. At T = 300 K, plate separations D < 8 Å result in a stable vapor bubble surrounded by liquid water of the enclosing bath. The hydrophobicity of the plates is responsible for this *shifting* of the phase equilibrium, as it favors the vapor by increasing the energy of confined liquid water.

(ii) In the confined system, liquid and vapor coexist in time, through *oscillations* between the two states, but not in space. While liquid and vapor in bulk can coexist in any proportion, the state in which liquid and a vapor bubble coexist in the nanoscopic volume between the plates is *unstable*. This can be seen in Figure 2 as a rapid passage from wet to dry plates, without dwelling in the intermediate, two-phase, states. Oscillations between liquid and vapor states have been previously observed in simulations of confined water.[21,35] What is distinct about the results shown in Figure 2 is the extent of the sampling that allows for a quantitative analysis of the thermodynamics and dynamics of this transition (see below).

(iii) There is a range of thermodynamic conditions, illustrated in Figure 2 by the distance D between the plates, for which transitions are observed between confined liquid and vapor. Tuning of the distance D between plates changes the fraction of time the confined system spends in the wet and dry states. The result, when an average over an ergodic trajectory of the system is taken, is an average density for confined water that changes continuously from the liquid to the vapor value as a function of D. Thus, the transition in the confined system is *first-order-like* and *rounded*. The plate separation for which the system has the same probability to be found in the liquid and vapor state is the equilibrium distance D_e, which we found to be comparable to the radius of the hydrophobic plates. The figure shows, however, that there is dynamical equilibrium between the two phases over a finite range of D around D_e.

While the time evolution of the density contains all the information needed for the analysis of the thermodynamics and kinetics of the phase transformation in the confined system, the quantification of the relative stability of the wet and dry states is more conveniently done in terms of the free energy. For the confined system, the potential of mean force corresponds to the grand canonical free energy Ω that we first evaluate using the density of the confined water as a reaction coordinate, $\Omega(\rho)$.

The free energy profiles $\Omega(\rho)$ for confined water at T = 330 K are presented in Figure 3 for the range of plate separations D

for which oscillations are observed between confined liquid and vapor states. The free energy profiles display two well-defined minima corresponding to the stable (or metastable) dry and wet states, over a range of plate separations of about 1 Å, from 7.9 to 9.1 Å. Beyond these plate separations, $\Omega(\rho)$ has a single stable minimum, and a single phase was observed in simulations lasting up to 400 ns. At $D_e = 8.5$ Å, the two confined phases have the same free energy. At this temperature, for any other plate separation, one of the phases is stable (liquid at $D > D_e$ and vapor at $D < D_e$), and the other is metastable. The disappearance of the metastable minimum in the free energy profile sets the effective limit of stability of the confined liquid and vapor states, the spinodal of the confined phases. The equilibrium coexistence line of nanoconfined vapor and liquid water has not been determined previously. The plate distances for which spontaneous drying was observed in other simulations, however, are in good agreement with the limit of stability of the liquid computed in this work: for a plate with radius $R_p = 8.8$ Å at $T = 300$ K we determine a liquid spinodal at 7.8 Å and a vapor spinodal at $D = 9$ Å; using the SPC/E model of water and the same hydrophobic disks and conditions, Berne and co-workers observed spontaneous drying at $D = 9.6$ Å[31] (and at $D = 10$ Å for same-sized repulsive ellipsoids[40]). Giovambattista et al. reported drying at $D = 8$ Å for SPC/E water confined between two hydrophobic square plates of about 30 Å length.[32] Although these and our results are comparable, we note that the details of the water−plate interaction potential and their size are relevant for a quantitative prediction of the liquid−vapor equilibrium in confined water.

The difference in free energy between the wet and dry state can be expressed by a simple capillary model based on macroscopic thermodynamics.[40] Writing the expressions for the grand potential of the confined liquid and vapor in terms of the surface energies between liquid and plate ($2\pi R_p^2\gamma_{lp}$), vapor and plate ($2\pi R_p^2\gamma_{vp}$), water in the liquid bath and confined vapor ($2\pi R_p D\gamma_{lv}$), and the corresponding pV term for each phase results in the following expression for the difference in grand canonical free energy between a confined vapor bubble of radius R_p and the confined liquid

$$\Delta\Omega = \Omega_v - \Omega_l \approx 2\pi R_p D\gamma_{lv} + [2\gamma_{lv}\cos\theta_{wp} + (p - p_v)D]\pi R_p^2 \quad (3)$$

where we have used Young's equation to relate the surface tensions of each phase with the plates to the contact angle between the liquid and plate and the liquid−gas surface tension, $\gamma_{lp} - \gamma_{vp} = -\gamma_{lv}\cos\theta_{wp}$, and have assumed that the bubble is cylindrical. In the stable vapor phase, the radius of the plate is approximately the radius of the bubble, $R_p \approx R_B$; otherwise R_p has to be replaced by the actual value of R_B in eq 3 above. This simple model predicts that the free energy gap between vapor and liquid $\Delta\Omega$ is linear with plate separation D, in agreement with the results of the simulations, plotted in Figure 4. At $D = 7.9$ Å, the free energy of the liquid is ∼15 kJ/mol higher than the vapor, and confined water is in the liquid state a mere 0.25% of the time; the opposite situation is observed for $D = 9.1$ Å. The D-range for which the system oscillates between liquid and vapor is given by the rate of change of the free energy difference with the plate separation, $(\partial\Delta\Omega/\partial D)_{R,T,\mu}$. The steepness of the free energy with plate separation determines the breadth of distances over which, for example, the system spends at least 1% of the time in the metastable phase. This corresponds to free energy differences within the range $0.01 \leqslant \exp(-\Delta\Omega/RT) \leqslant 100$. The macroscopic thermodynamic model of eq 3 predicts that the D-range of metastability decreases rapidly with increasing size of the plates. This is, indeed, what is observed in the simulations: at $T = 300$ K, the range dynamical coexistence is $\Delta D = 1.2$ Å for $R_p = 8.8$ Å and $\Delta D = 1.9$ Å for a smaller plate with $R_p = 6.7$ Å. The scaling suggests that for plates larger than about 5 nm diameter the range of plate distances over which the confined system presents bistability between a stable and metastable phase may be insignificant.

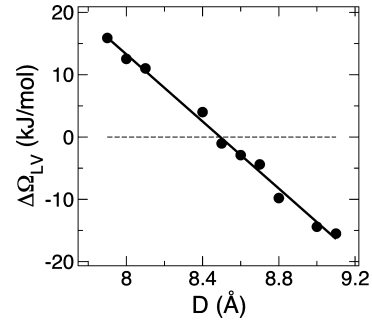

Figure 4. Free energy difference $\Delta\Omega(\rho)$ between liquid (wet) and vapor (dry) states as a function of plate separation for water confined by the $R_p = 8.8$ Å hydrophobic plates at 330 K. The confined system is immersed in a bath of liquid water at 330 K and 1 atm. The circles show the actual data and the line a linear fit. A linear free energy gap as a function of plate separation is predicted by eq 3.

The small D range over which oscillations between the two phases are observed for the plate of radius $R_p = 8.8$ Å may suggest that the oscillatory behavior could be suppressed by allowing the atoms in the plate to vibrate with an amplitude of about 0.5 Å. To investigate this possibility, we performed simulations on a system for which the particles of the plates were not fixed but tethered through soft harmonic springs (with spring constant $k_s = 5$ kcal/Å^2 mol) to their initial in-plane positions. The particles of the plate vibrate with an amplitude of about 0.5 Å and standard deviation of the positions perpendicular to the plate $[\langle z^2\rangle - \langle z\rangle^2]^{1/2} = 0.35$ Å. We found that the equilibrium distance D_e of the rigid and fluctuating plates was within 0.1 Å of each other and that the D-range of stability of the liquid and vapor was around 1 Å for the two cases. We conclude that realistic vibration of the atoms of the hydrophobic surface does not significantly affect the oscillatory equilibrium and the range in which dynamical coexistence is observed. This is different from what Andreev et al. found for water confined in narrow carbon nanotubes.[26] When water fills the nanotube, it forms a single file of hydrogen bonded water molecules. The simulations of ref 26 indicate that an increase in flexibility of the tube leads to a squeezing of the confined water by forcing the molecules into an energetically unfavorable straight arrangement. There is no such constraint for water confined between two disks when these are made flexible.

The stable liquid and vapor states in Figure 3 are separated by a free energy maximum at $\rho/\rho_o \approx 0.43$, which corresponds to a vapor bubble that occupies about half the available volume between the plates. The work needed to open a bubble of radius R_B in the liquid state is given by eq 3 which predicts a quadratic dependence of $\Delta\Omega$ on the radius of the vapor bubble. The two minima are the stable vapor and liquid states of Figure 3. If the density of water between the plates was the proper reaction coordinate for the phase transformation, then the maximum in $\Omega(\rho)$ would signal the transition states for the liquid to vapor transition. Figure 5 shows the free energy barrier $\Delta\Omega^{\#}$ from the liquid to the top as a function of the plate separation D, for the phase equilibria at $T = 330$ K. We find that $\Delta\Omega^{\#}$ has a

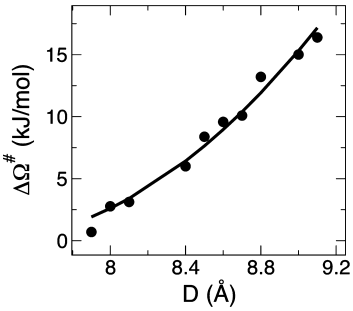

Figure 5. Free energy barrier $\Delta\Omega(\rho)^{\#}$ between wet (liquid) and dry (vapor) states as a function of the separation between the confining plates of radius 8.8 Å at 330 K. The confined system is immersed in a bath of liquid water at 330 K and 1 atm. The circles are the data obtained from the simulations and the line a fit to a quadratic function.

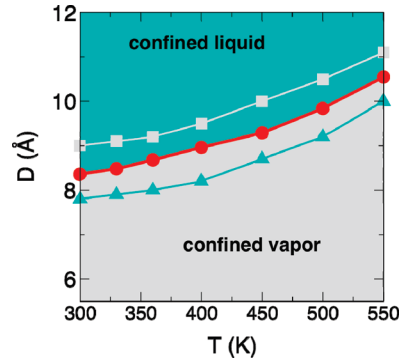

Figure 6. Phase diagram of $D-T$ for water between the hydrophobic plates of radius $R_p = 8.8$ Å immersed in a bath of liquid water at $p =$ 1 atm and temperature T. The equilibrium separation $D_e(T)$ (red circles) separates the regions of stability of the liquid (turquoise) and vapor (gray), and it is flanked by the spinodal lines that demark the limit of stability of the liquid (turquoise line with triangles) and the vapor (gray line with squares).

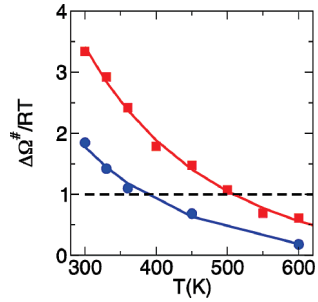

Figure 7. Free energy barrier $\Delta\Omega(\rho)^{\#}$, divided by the thermal energy RT, along the coexistence line between dry and wet states. The confined system is in contact with a bath of liquid water at $p = 1$ atm and temperature T. The free energy barrier decreases with increasing temperature. For the plates of radius $R_p = 8.8$ Å, the free energy barrier becomes smaller than the thermal energy for $T > 500$ K. For a smaller plate with $R_p = 6.7$ Å, the barrier is ~1.9 times lower, consistent with the scaling of R_p^2 predicted by eq 3, and the barrier becomes equal to the thermal energy already around 360 K.

nonlinear, quadratic dependence with D. Berne and co-workers have shown that an approximately quadratic dependence of the barrier $\Delta\Omega^{\#}$ on the plate separation is expected from eq 3 when the D dependence of the radius of the vapor bubble at the top of the barrier is taken into account.[40] A quadratic relation was previously deduced by Lum and Chandler, who considered that if water cannot access the full volume of the plates and the last term dominates in eq 3 then the activation barrier should scale with $(D - 2\delta)^2$, where δ is the distance from the center of each plate that is inaccessible to water.[41] There are, in principle, two contributions to δ: the finite size of the water−plate interaction and predrying (the formation of a vapor layer between the liquid and plate).[41] Liquid water with significantly diminished density over a distance of about 1−6 Å from hydrophobic surfaces has been deduced from X-ray and neutron reflectivity experiments of *large* surfaces.[42−44] The solid line in Figure 5 shows the best fit of the results of the simulation to $\Delta\Omega^{\#} = c(D - 2\delta)^2$, for which $\delta = 3.65$ Å. This is essentially identical to the water−plate distance parameter, $\sigma_{wp} = 3.56$ Å, thus indicating that predrying does not occur for water confined in the small hydrophobic plates of this study. The absence of a vapor layer between liquid and hydrophobic plates with dimensions about 1.5 nm in diameter has also been reported in ref 21.

We now turn our focus to the temperature dependence of the oscillatory equilibrium, with the goal of constructing the phase diagram $D-T$ for water confined between the hydrophobic disks in contact with a bath of liquid water at T and $p = 1$ atm. We performed extensive simulations varying the plate separation at temperatures up to 600 K, where the water bath is in a superheated liquid state (but before its cavitation limit, about 850 K for mW water at 1 atm[45]). The equilibrium distance D_e for each temperature and the corresponding limits of stability of the liquid and vapor states are displayed in the phase diagram of Figure 6. To the best of our knowledge, the equilibrium lines and liquid and vapor spinodals of water in hydrophobic nanoconfinement have not been previously reported in the literature. The region of dynamical coexistence between the liquid and vapor, determined by the corresponding phase limits, does not change significantly in this temperature range. Note that while the region of dynamic coexistence is not wide in D it is quite wide in terms of the temperatures. At $D = 8.75$ Å, for example, liquid−vapor oscillations occur over a range of temperatures wider than 100 K. The T-range of bistability is controlled by the steepness in the change of free energy difference between liquid and vapor with temperature, $(\partial\Delta\Omega/\partial T)_{R,D}$. According to eq 3, this is modulated by the temperature dependence of the liquid−vapor surface tension, $(\partial\gamma_{lv}/\partial T)_V$. We note that the surface tension of mW water agrees with experiment at 360 K, while it is 92% of the experimental value at 298 K;[36] thus, we expect a similar, but slightly smaller, T-range of liquid−vapor dynamic coexistence in experiments with similar hydrophobic nanoscopic plates.

The equilibrium separation D_e increases with temperature because heating increases the stability of large vapor bubbles, allowing for larger plate separations before the liquid sets in. The frequency of the liquid−vapor oscillations at D_e also increases with temperature, not only because the system has more thermal energy to surmount the free energy barrier $\Delta\Omega^{\#}$ but mainly because the barrier itself decreases, as shown in Figure 7. The decrease in $\Delta\Omega^{\#}$ is associated with the decrease of the liquid−vapor surface tension as water approaches its bulk critical point (that for mW water is located around $T_c \approx 925$ K and $p_c \approx 13.4$ MPa[45]). The figure also shows the barriers at equilibrium for a smaller plate with radius $R = 6.7$ Å. $\Delta\Omega^{\#}$ increases with the size of the plate because the maximum of the barrier corresponds to a larger bubble that has a lower probability of formation. The ratio of the barrier for the large and small plates is ~1.9 for all temperatures. This is the ratio expected if $\Delta\Omega^{\#}$ scales with R^2, as predicted by eq 3.

To quantify the kinetics of the phase transformation, we computed the probability that the liquid (vapor) survives for at least a time t, before transforming to vapor (liquid). Using the

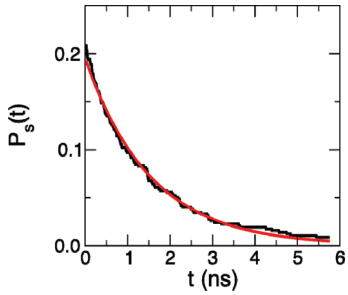

Figure 8. The survival probability $P_s(t)$ of the liquid between the plates of radius $R_p = 8.8$ Å at a distance $D = 8.4$ Å and temperature $T = 300$ K (black line) is well represented by a single exponential with a characteristic time of 1.6 ns (red curve). The survival probability in this plot starts at around 0.2 because about 80% of the trajectories that reach the density that corresponds to the top of the free energy barrier $\Omega(\rho)^{\#}$ return to their original state within 10 ps.

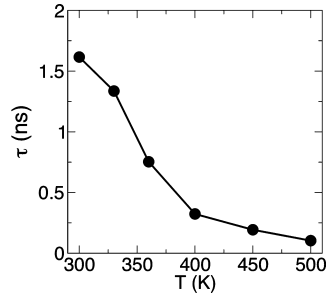

Figure 9. Characteristic survival time of the liquid at the equilibrium plate separation close to D_e as a function of the temperature. The confined system is immersed in a bath of liquid water at $p = 1$ atm and temperature T. The characteristic time at 300 K is lower than it would appear from the extrapolation of the higher temperature values because the thermodynamic conditions slightly favored the vapor state.

density of the confined phase as a reaction coordinate, we used the top of the free energy barrier to divide the phase space into liquid and vapor regions. We consider that a system crossed from liquid (vapor) to vapor (liquid) if the density reached $\rho^{\#}/\rho_o - (+)\ \delta\rho/\rho_o$, and the purpose of the extra $\delta\rho/\rho_o = 0.03$ in each direction is to avoid counting the reaching of the barrier as a transition. A typical survival probability plot is shown in Figure 8. We find that about 80% of the barrier crossings result in immediate return within less than 10 ps, without the system reaching the basin on the other side (see central panel of Figure 2, for which the system diffuses back and forth along the top of the barrier, $\rho^{\#}/\rho_o = 0.45$). This suggests that knowledge of the density ρ of confined water does not suffice to determine precisely the transition state; there are other coordinates that are relevant to the pathway of the phase transformation. The survival times of the transitions that do not result in immediate return follow single exponential decays. At the equilibrium distance D_e, the characteristic time τ of liquid and vapor is the same and decreases with temperature from about 2 ns at 300 K to 0.1 ns at 500 K (Figure 9). Note that at $T = 500$ K for the plates of radius $R_p = 8.8$ Å and at 360 K for the smaller plates the barrier $\Delta\Omega^{\#}$ reaches the thermal energy RT, $\Delta\Omega^{\#}/RT = 1$; beyond these temperatures, the transitions are so fast that the time scale for the fluctuations between states become comparable to the relaxation time within a state.

The characteristic times computed from the distribution of survival times in the simulations, τ, can be compared with the predictions of transition state theory[46–48] for which we use the free energy barriers computed from the simulations, assuming that the density of the confined system was the reaction coordinate of the liquid−vapor transformation

$$\tau^{TST} = \tau_o \exp(\Delta\Omega^{\#}/RT) \quad (4)$$

Use of the gas phase expression $\tau_o = h/kT$ (where h is Planck's and k is Boltzmann's constant) for the rate calculation of the phase transformation in the nanoscopic system results in a τ^{TST} 2 orders of magnitude shorter than the actual time measured from the analysis of the survival times in the simulations. A more appropriate preexponent for the calculation of the rate in a condensed phase would be $\tau_o = 2\pi/\omega_r$, where the frequency ω_r is obtained from the curvature of the PMF well for the "reactant" phase (e.g., the PMF of the liquid, in the liquid to vapor transition) by approximating the bottom of the reactant's free energy well to a harmonic potential.[48] We do not attempt a quantitative comparison with TST using $\tau_o = 2\pi/\omega_r$ because it is nontrivial to compute the reduced mass m (note that m does not have mass units when ρ/ρ_o is the reaction coordinate), and it has also been demonstrated in ref 49 that an additional correction factor should be considered for non-Cartesian reaction coordinates such as ρ/ρ_o. Instead, we look at the unsuccessful recrossings of the system over the top of the free energy barrier, evident in the inability of ~80% of the trajectories that reach the barrier to cross it successfully toward the "product" phase. These suggest a transmission coefficient $\kappa = \tau^{TST}/\tau$ still much lower than 1 (but not as low as the 0.01 suggested by a naïve use of the gas state expression for the frequency). This scenario is consistent with Kramer's expression of TST under conditions for which the "solvent" slows the dynamics along the reaction coordinate by virtue of exerting a friction on it.[50] The "solvent", in this case, refers to all water coordinates except ρ, including the coordinates from the water bath outside the plates. Leung and Luzar studied the dynamics of capillary evaporation of a lattice gas model using Monte Carlo and umbrella sampling to construct the free energy curves as a function of the vapor bubble size (equivalent to the bubble area); they computed the transmission coefficients from the top of that free energy barrier and found transmission coefficients around 0.4.[51] The high fraction of unsuccessful trajectories evident in Figures 3 and 8 suggests that κ may be smaller for the plates of the present study. A low transmission coefficient that arises from strong coupling of the density of confined water to other coordinates of the confined and bath molecules should not be surprising because, given that the number of water molecules between our $R_p = 8.8$ Å plates is in the order of 30−40 at $\rho^{\#}$, it may be expected that individual fluctuations in the positions of a few molecules could have a strong effect on the fate of the vapor bubble at the top of $\Omega(\rho)$, even if they do not affect significantly the number of molecules between the plates.

To obtain more insight on the evolution of the vapor bubble in the transformation between liquid and vapor states, we considered two additional collective coordinates for the confined system: the area A and perimeter L of the vapor bubble. We found that the bubble area A and density of the confined water ρ are correlated, confirming that the transition states consist of an intermediate size bubble coexisting with a dense liquid and not a homogeneous gas of intermediate density (this was also verified by the visualization of the position of the water molecules in the confined volume along the simulation trajectories). As density and bubble area are correlated, the latter does not provide an additional independent coordinate to describe the transformation between liquid and vapor. The perimeter L of the bubble, on the other hand, is not trivially related to its area or the density, except if the shape of the bubble is fixed (e.g., perfectly cylindrical, as assumed in the simple model described by eq 3). Figure 10 shows the potential of mean force

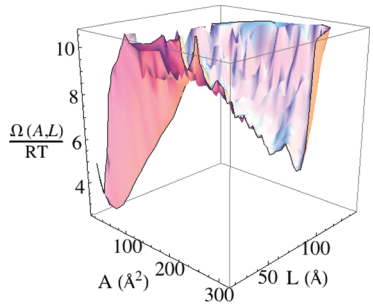

Figure 10. Potential of mean force for water confined between hydrophobic plates of radius $R_p = 8.8$ Å at distance $D = 8.4$ Å and temperature $T = 300$ K (in contact with a bath of liquid water at 300 K and 1 atm) as a function of area A and perimeter L of the vapor bubble, $\Omega(A,L)$. The barrier from liquid to saddle point is 7.5 kJ/mol, comparable to the 8.8 kJ/mol computed from the one-dimensional $\Omega(\rho)$ at the same conditions. The vapor basin is much broader than the liquid one because the vapor bubble adopts a broad range of perimeters L for a given area A.

as a function of A and L obtained from the trajectory at $T = 300$ K and $D = 8.4$ Å. The free energy $\Delta\Omega(A,L)$ presents a narrow well for the liquid state (more stable than the vapor under these conditions) connected by a shallow saddle point to a broader well corresponding to the vapor phase. An analysis of the relation between the area and perimeter of the bubble indicates that the larger the bubble, the more pronounced are its fluctuations in shape. This is observed in the breadth of L values observed for each value of A in the vapor basin. For the vapor state, these originate in the attempt of the liquid to wet the rim of the plates, as shown in the top left panel of Figure 3. The free energy barrier measured from the bottom of the liquid free energy well to the saddle point is $\Delta\Omega(A,L)^{\#}$ is ~7.5 kJ/mol. This is comparable to the barrier obtained by considering the density alone, $\Delta\Omega(\rho)^{\#} = 8.8$ kJ/mol, for the same simulation trajectory. We observe a lower number of recrossings of the top of the barrier when both the area and the perimeter of the bubble are used as reaction coordinates. Figure 11 shows L vs A for two representative 10 ns pieces of the 400 ns trajectory used to construct the PMF of Figure 10. The large circle indicates the position of the saddle point, $\Delta\Omega(A,L)^{\#}$. In most successful transformations, the vapor bubble has dimensions close to those corresponding to the top of the free energy barrier (we call these $A^{\#}$ and $L^{\#}$). Consistent with the broad transition region in the PMF of Figure 10, there is a range of perimeters for which the bubble successfully crosses from the liquid to the vapor state. The lower panel of Figure 10 shows, however, that vapor bubbles with a relatively large L/A ratio do not succeed in producing a transition to the basin of the vapor state, although they reach the critical area $A^{\#}$. As the area of the vapor bubble and density of the confined water are linearly related, this indicates that the large number of recrossings of the top of the barrier while using ρ/ρ_o as the only reaction coordinate was due, mainly, to the formation of bubbles with large perimeter, i.e., bubbles that strongly depart from a cylindrical shape.

Conclusions

In this work, we have used extensive molecular dynamics simulations to characterize the thermodynamics and dynamics of the liquid−vapor (wetting−drying) transition of water confined between nanoscopic hydrophobic plates immersed in a bath of liquid water at normal pressure. The liquid−vapor equilibrium of water confined in a nanoscopic volume presents several differences with the liquid−vapor equilibrium in bulk

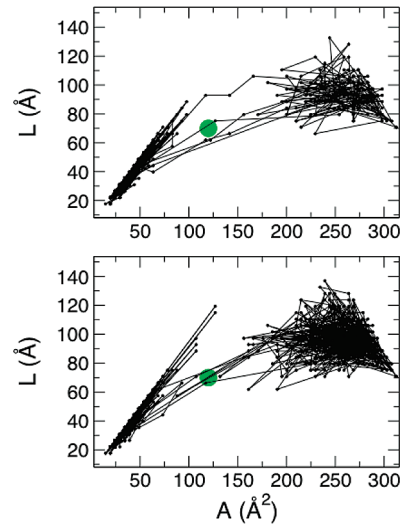

Figure 11. Time evolution of the area A and perimeter L of the largest vapor bubble for water confined between hydrophobic plates of radius $R_p = 8.8$ Å at distance $D = 8.4$ Å and temperature $T = 300$ K. The confined system is immersed in a bath of liquid water at 1 atm and 300 K. Each panel shows the evolution of the largest bubble for a representative 10 ns piece of the 400 ns trajectory (contiguous times connected by lines, configurations indicated by a small black circle). The large green circle indicates the position of the saddle point in the free energy profile, $\Omega(A,L)^{\#}$. In the piece of the trajectory shown in the upper panel, bubbles that reach the critical area $A^{\#}$ successfully transition to the other phase. The lower panel illustrates cases in which bubbles successfully cross the transition state region and also displays cases in which bubbles that originate in the liquid reach the critical area $A^{\#}$ and a perimeter L that is much larger than $L^{\#}$, and the bubble closes again. If only the bubble area (or, equivalently, the density of the confined water) is considered in the analysis of the mechanism, these latter trajectories would contribute to decrease the transmission coefficient.

water. First, the equilibrium temperatures can be shifted through control of the water−surface interactions. Drying at ambient temperatures, where bulk water is a stable liquid, can be attained by increasing the hydrophobicity of the interface.[21] A water−surface contact angle larger than 90° is a necessary condition to observe wetting−drying transitions in open nanoscopic systems immersed in a stable liquid water bath, and a strong sensibility of this transition to water−surface attraction has been previously reported in the literature.[21,26,33]

A second and more fundamental difference between the liquid−vapor transition in bulk and nanoconfinement is in the nature of phase coexistence. This has been the focus of this study. Different from bulk water, spatial coexistence of liquid and vapor is not possible for water confined in a nanoscopic volume. The two-phase confined system is *unstable* with respect to all-liquid or all-vapor states. This is due to the unfavorable surface energy between confined liquid and vapor. The surface free energy represents an important contribution to the free energy of the nanoscopic system, but it is negligible in a bulk system. In nanoconfined water, the two phases coexist in time through oscillations but do not coexist in space, except transiently as the confined water transitions between liquid and vapor. The characteristic time of the oscillations in equilibrium is controlled by the free energy cost of the interface between confined liquid and vapor. This free energy barrier increases with the size of the plates and the surface tension (thus models that strongly underestimate the surface tension of water produce faster transitions between wet and dry states, such as the case for the transitions observed in TIP3P water[35] that at room temperature has a γ_{lv} 30% lower than in experiments[52]). The

larger the plates, the rarer is the fluctuation that produces a bubble of size sufficient to tip the system to the other phase. We investigated the dynamics of the phase transformation in terms of (i) the density of the confined liquid ρ as the reaction coordinate and (ii) the area A and perimeter L of the largest vapor bubble present between the plates as reaction coordinates. If only ρ (or, equivalently, A) is used, crossing from liquid to vapor requires several uncorrelated attempts in which the system reaches $\rho^{\#}$ (or $A^{\#}$) but nevertheless returns to the liquid state. An analysis of the evolution in terms of L and A shows that most of these apparent recrossings are related to the formation of bubbles that are destabilized by a large perimeter for their area. The use of area and perimeter of the bubble as reaction coordinates diminishes but does not completely eliminate the unsuccessful crossings of the transition region in $\Omega(A, L)$. We interpret the remaining recrossings as arising from the friction due to the solvent (i.e., all coordinates not used for the PMF, including the bath's coordinates). A more thorough study including committor analysis[53] and the calculation of the transmission coefficients around the top of the free energy barrier[51] is beyond the scope of this study, but it is necessary to identify the actual transition states for the liquid−vapor transition of water confined between hydrophobic plates.

A third difference between nanoconfined and bulk water is the existence of reversible transitions between a stable and a metastable state over a range of thermodynamic conditions. We computed the $D-T$ phase diagram of confined water: the equilibrium $D_e(T)$ and the limits of stability of each confined phase that determine the range of plate distances (ΔD) and temperatures (ΔT) over which liquid and vapor coexist in dynamical equilibrium. To the best of our knowledge, this is the first report of the equilibrium and spinodal lines for confined water. The location of the coexistence and spinodal lines depends on the size of the plates and their hydrophobicity. For the plate sizes of this study, with radius 6.7 and 8.8 Å, ΔD was around 2 and 1 Å, respectively, and we found that the oscillations were not significantly affected if the atoms of the plate were allowed to vibrate. The ΔT for which oscillations were observed at constant D is quite broad, more than 100 K for the largest plate of this study. The magnitudes of ΔD and ΔT are controlled by the rate of change of the free energy difference between liquid and vapor with D or T, respectively. A simple macroscopic thermodynamic (capillary) model predicts that both ΔD and ΔT should be a strong decreasing function of the size of the confining plates, thus we do not expect liquid−vapor oscillations for plates with radii that extend beyond a few nanometers.

The oscillations in nanoconfined water occur under conditions of phase equilibrium (when the free energy of the two phases is the same) and also within a finite range of the thermodynamic variables around equilibrium where the system oscillates between a stable and a metastable state. This situation is never observed in bulk because the critical nucleus to form the new phase at equilibrium is macroscopic, while the fluctuations that produce the structure of the new phase (i.e., the nuclei) are microscopic. A large superheating of the liquid (supercooling of the vapor) is needed to homogeneously nucleate the bulk vapor (liquid); after the transformations occur under these conditions of high driving force, the system cannot return to the metastable state because the barrier is unsurmountable. In this respect, the phase transition in confinement resembles its bulk counterpart less than the isomerization of a relatively large molecule immersed in solvent. The characteristic survival time of each phase in equilibrium is about 2 ns for the $R_p = 8.8$ Å plates at room temperature. As the free energy barrier that separates the two states in equilibrium increases approximately with R_p^2 (actually faster, because D_e also increases with R_p), the characteristic survival times are expected to increase rapidly with plate size. Extrapolating from the τ measured in the small plates of this study, we expect, for example, that the survival time for plates of 35 Å diameter will be about 100 ns. We note, however, that knowledge of the free energy barrier is insufficient for a quantitative prediction of the rates, as the confined water experiences recrossings at the top of the barrier that decrease the actual transition rates. We ascribe the increase in τ to the effect of the friction of the "solvent" coordinates (including those of the bath) on the area (or confined system's density) and perimeter of the bubble.

In this work, we focused on the liquid−vapor transition in nanoconfined water and found that the nature of phase coexistence differs from that of bulk water. How general are the conclusions of this study to other phase transitions and substances? The oscillations between confined vapor and liquid water are a signature of the small size of the confined system, as they are related to a positive and non-negligible interfacial contribution to the free energy of the coexisting system.[54–57] We suggest that the coexistence through oscillations that we report for the wetting−drying transition of water between hydrophobic plates is closely related to the dynamical coexistence in liquid−crystal and crystal−crystal transformations previously reported for small atomic and molecular clusters under canonical and microcanonical conditions.[56,57] The main differences between the clusters and the nanoconfined systems of this study are that the liquid−vapor transitions occur in open (grand canonical) nanoscopic systems and that the nanoconfined water is itself stable, while free-standing clusters are metastable with respect to evaporation. We expect the results of this study to be general for other transitions of water in open systems, such as the liquid−ice and ice−vapor transitions for water confined between nanoscopic disks similar to those in this study. Liquid−ice oscillations indeed can occur in nanoconfined water and are presented in a separate communication.[58] Phase coexistence in time but not in space is not restricted to water; while there have been some studies of dynamic coexistence in small free-standing water clusters,[59–61] most have been performed for rare gas and metallic systems, usually modeled with Lennard-Jones potentials.[54–57] For liquid−vapor oscillations to occur in a confined system open to its own stable liquid, however, the plates have to be nonwetting (i.e., present contact angle larger than 90°) for the liquid of interest. This condition occurs for water on hydrophobic surfaces, but it may not be easy to attain for other substances. Moreover, water has a central function in materials and biology that is unparalleled by other liquids. As hydrophobic cavities of a size comparable to those considered in this study could occur in nanofluidic devices and polymer membranes, the results of this study prompt the question of whether the existence of wetting−drying oscillations with a time scale on the order of nanoseconds has an impact in the molecular transport, stability, or function of these materials.

Acknowledgment. We thank Srabani Taraphder for fruitful discussions and Liam Jacobson for rendering Figure 10. V.M. gratefully acknowledges the National Science Foundation for partial support of this work through Collaborative Research Grant NSF CHE-0628257. L.X. acknowledges support from World Premier International Research Center Initiative (WPI Initiative), MEXT, Japan. We thank the Center of High Performance Computing at the University of Utah for allocation of computing time.

References and Notes

(1) Chandler, D. *Nature* **2005**, *437*, 640.
(2) Berne, B.; Weeks, J.; Zhou, R. *Annu. Rev. Phys. Chem.* **2009**, *60*, 85.
(3) Rasaiah, J.; Garde, S.; Hummer, G. *Annu. Rev. Phys. Chem.* **2008**, *59*, 713.
(4) Ball, P. *ChemPhysChem* **2008**, *9*, 2677.
(5) Beckstein, O.; Sansom, M. *Proc. Natl. Acad. Sci.* **2003**, *100*, 7063.
(6) Findenegg, G. H.; Jaehnert, S.; Akcakayiran, D.; Schreiber, A. *ChemPhysChem* **2008**, *9*, 2651.
(7) Koga, K.; Gao, G. T.; Tanaka, H.; Zeng, X. C. *Nature* **2001**, *412*, 802.
(8) Koga, K.; Gao, G. T.; Tanaka, H.; Zeng, X. C. *Phys. A (Amsterdam, Neth.)* **2002**, *314*, 462.
(9) Koga, K.; Parra, R. D.; Tanaka, H.; Zeng, X. C. *J. Chem. Phys.* **2000**, *113*, 5037.
(10) Koga, K.; Tanaka, H. *J. Chem. Phys.* **2005**, *122*, 104711.
(11) Koga, K.; Zeng, X.; Tanaka, H. *Phys. Rev. Lett.* **1997**, *79*, 5262.
(12) Bai, J.; Zeng, X. C.; Koga, K.; Tanaka, H. *Mol. Simul.* **2003**, *29*, 619.
(13) Koga, K.; Tanaka, H.; Zeng, X. C. *Nature* **2000**, *408*, 564.
(14) Slovak, J.; Tanaka, H.; Koga, K.; Zeng, X. C. *Phys. A (Amsterdam, Neth.)* **2003**, *319*, 163.
(15) Zangi, R.; Mark, A. E. *J. Chem. Phys.* **2003**, *119*, 1694.
(16) Kimmel, G. A.; Matthiesen, J.; Baer, M.; Mundy, C. J.; Petrik, N. G.; Smith, R. S.; Dohnalek, Z.; Kay, B. D. *J. Am. Chem. Soc.* **2009**, *131*, 12838.
(17) Stacchiola, D.; Park, J. B.; Liu, P.; Ma, S.; Yang, F.; Starr, D. E.; Muller, E.; Sutter, P.; Hrbek, J. *J. Phys. Chem. C* **2009**, *113*, 15102.
(18) Maniwa, Y.; Kataura, H.; Abe, M.; Suzuki, S.; Achiba, Y.; Kira, H.; Matsuda, K. *J. Phys. Soc. Jpn.* **2002**, *71*, 2863.
(19) Maniwa, Y.; Kataura, H.; Abe, M.; Udaka, A.; Suzuki, S.; Achiba, Y.; Kira, H.; Matsuda, K.; Kadowaki, H.; Okabe, Y. *Chem. Phys. Lett.* **2005**, *401*, 534.
(20) Johnston, J. C.; Kastelowitz, N.; Molinero, V., manuscript in preparation.
(21) Choudhury, N.; Pettitt, B. M. *J. Am. Chem. Soc.* **2007**, *129*, 4847.
(22) Berne, B.; Weeks, J.; Zhou, R. *Annu. Rev. Phys. Chem.* **2009**, *60*, 85.
(23) Hua, L.; Huang, X.; Liu, P.; Zhou, R.; Berne, B. *J. Phys. Chem. B* **2007**, *111*, 9069.
(24) Hua, L.; Zangi, R.; Berne, B. J. *J. Phys. Chem. C* **2009**, *113*, 5244.
(25) Liu, P.; Huang, X.; Zhou, R.; Berne, B. J. *Nature* **2005**, *437*, 159.
(26) Andreev, S.; Reichman, D.; Hummer, G. *J. Chem. Phys.* **2005**, *123*, 194502.
(27) Hummer, G.; Rasaiah, J.; Noworyta, J. *Nature* **2001**, *414*, 188.
(28) Rasaiah, J.; Garde, S.; Hummer, G. *Annu. Rev. Phys. Chem.* **2008**, *59*, 713.
(29) Kastelowitz, N.; Johnston, J. C.; Molinero, V. *J. Chem. Phys.* **2010**, *132*, 124511.
(30) Choudhury, N.; Pettitt, B. M. *J. Am. Chem. Soc.* **2007**, *129*, 4847.
(31) Zangi, R.; Hagen, M.; Berne, B. J. *J. Am. Chem. Soc.* **2007**, *129*, 4678.
(32) Giovambattista, N.; Rossky, P. J.; Debenedetti, P. G. *Phys. Rev. E* **2006**, *73*, 041604.
(33) Hummer, G.; Rasaiah, J. C.; Noworyta, J. P. *Nature* **2001**, *414*, 188.
(34) Patashinski, A.; Ratner, M. *Phys. Rev. E* **2008**, *78*, 041106.
(35) England, J. L.; Pande, V. S.; Haran, G. *J. Am. Chem. Soc.* **2008**, *130*, 11854.
(36) Molinero, V.; Moore, E. B. *J. Phys. Chem. B* **2009**, *113*, 4008.
(37) Stillinger, F. H.; Weber, T. A. *Phys. Rev. B* **1985**, *31*, 5262.
(38) Plimpton, S. J. *J. Comput. Phys.* **1995**, *117*, 1.
(39) Plimpton, S. J. Available online at lammps.sandia.gov, 2005.
(40) Huang, X.; Margulis, C.; Berne, B. *Proc. Natl. Acad. Sci. U.S.A.* **2003**, *100*, 11953.
(41) Lum, K.; Chandler, D. *Int. J. Thermophys.* **1998**, *19*, 845.
(42) Mezger, M.; Schoeder, S.; Reichert, H.; Schroeder, H.; Okasinski, J.; Honkimaeki, V.; Ralston, J.; Bilgram, J.; Roth, R.; Dosch, H. *J. Chem. Phys.* **2008**, *128*, 244705.
(43) Poynor, A.; Hong, L.; Robinson, I. K.; Granick, S. *Phys. Rev. Lett.* **2006**, *97*, 4.
(44) Maccarini, M.; Steitz, R.; Himmelhaus, M.; Fick, J.; Tatur, S.; Wolff, M.; Grunze, M.; Janecek, J.; Netz, R. R. *Langmuir* **2007**, *23*, 598.
(45) Xu, L.; Molinero, V., in preparation.
(46) Eyring, H. *J. Chem. Phys.* **1935**, *3*, 63.
(47) Chandler, D. *J. Chem. Phys.* **1978**, *68*, 2959.
(48) Pollak, E.; Talkner, P. *Chaos* **2005**, *5*, 026116.
(49) Schenter, G.; Garrett, B.; Truhlar, D. *J. Chem. Phys.* **2003**, *119*, 5828.
(50) Kramers, H. *Physica* **1940**, *7*, 284.
(51) Leung, K.; Luzar, A. *J. Chem. Phys.* **2000**, *113*, 5845.
(52) Vega, C.; de Miguel, E. *J. Chem. Phys.* **2007**, *126*, 154707.
(53) Bolhuis, P. G.; Chandler, D.; Dellago, C.; Geissler, P. L. *Annu. Rev. Phys. Chem.* **2002**, *53*, 291.
(54) Berry, R. S. *Theory of Atomic and Molecular Clusters*; Jellinek, J., Ed.; Springer: Berlin, 1999.
(55) Berry, R. S.; Smirnov, B. A. *Int. J. Mass Spectrom.* **2009**, *280*, 204.
(56) Kunz, R.; Berry, R. *Phys. Rev. E* **1994**, *49*, 1895.
(57) Wales, D.; Berry, R. *Phys. Rev. Lett.* **1994**, *73*, 2875.
(58) Kastelowitz, N.; Molinero, V. To be submitted.
(59) Wales, D.; Ohmine, I. *J. Chem. Phys.* **1993**, *98*, 7245.
(60) Laria, D.; Rodriguez, J.; Dellago, C.; Chandler, D. *J. Phys. Chem. A* **2001**, *105*, 2646.
(61) Nishio, K.; Mikami, M. *J. Chem. Phys.* **2009**, *130*, 154302.

JP102443M